Journal of Biomedical Optics

BiomedicalOptics.SPIEDigitalLibrary.org

Molecular imaging of human tumor cells that naturally overexpress type 2 cannabinoid receptors using a quinolone-based near-infrared fluorescent probe

Zhiyuan Wu
Pin Shao
Shaojuan Zhang
Xiaoxi Ling
Mingfeng Bai

SPIE.

Molecular imaging of human tumor cells that naturally overexpress type 2 cannabinoid receptors using a quinolone-based near-infrared fluorescent probe

Zhiyuan Wu,[a,b,†] Pin Shao,[a,†] Shaojuan Zhang,[a,c] Xiaoxi Ling,[a] and Mingfeng Bai[a,d,e,*]
[a]University of Pittsburgh, Molecular Imaging Laboratory, Department of Radiology, Pittsburgh, Pennsylvania 15219
[b]Shanghai Jiao Tong University School of Medicine, Ruijin Hospital, Department of Radiology, Shanghai 200025, China
[c]Xi'an Jiaotong University, The First Hospital of Medical School, Department of Diagnostic Radiology, Xi'an, Shaanxi 710061, China
[d]University of Pittsburgh Cancer Institute, Pittsburgh, Pennsylvania 15232, United States
[e]University of Pittsburgh, Department of Bioengineering, Pittsburgh, Pennsylvania 15232, United States

Abstract. Cannabinoid CB2 receptors (CB_2R) hold promise as therapeutic targets for treating diverse diseases, such as cancers, neurodegenerative diseases, pain, inflammation, osteoporosis, psychiatric disorders, addiction, and immune disorders. However, the fundamental role of CB_2R in the regulation of diseases remains unclear, largely due to a lack of reliable imaging tools for the receptors. The goal of this study was to develop a CB_2R-targeted molecular imaging probe and evaluate the specificity of the probe using human tumor cells that naturally overexpress CB_2R. To synthesize the CB_2R-targeted probe (NIR760-Q), a conjugable CB_2R ligand based on the quinolone structure was first prepared, followed by bioconjugation with a near-infrared (NIR) fluorescent dye, NIR760. *In vitro* fluorescence imaging and competitive binding studies showed higher uptake of NIR760-Q than free NIR760 dye in Jurkat human acute T-lymphoblastic leukemia cells. In addition, the high uptake of NIR760-Q was significantly inhibited by the blocking agent, 4-quinolone-3-carboxamide, indicating specific binding of NIR760-Q to the target receptors. These results indicate that the NIR760-Q has potential in diagnostic imaging of CB_2R positive cancers and elucidating the role of CB_2R in the regulation of disease progression. [DOI: 10.1117/1.JBO.19.7.076016]

Keywords: CB_2 receptor; near-infrared; optical imaging; leukemia; fluorescence imaging.

Paper 140095R received Feb. 17, 2014; revised manuscript received Apr. 24, 2014; accepted for publication May 1, 2014; published online Jul. 18, 2014.

1 Introduction

Since its discovery in 1993, an increasing amount of effort has been invested in studying the pharmacology and physiopathological role of type 2 cannabinoid receptors (CB_2R). Presently, both academia and the pharmaceutical industries consider this receptor as a major therapeutic target. Specifically, CB_2R represents a promising target to treat inflammation,[1,2] pain,[3] osteoporosis,[4] autoimmune diseases,[5] addiction,[6,7] psychiatric disorders,[8–10] diabetes,[11–13] cardiovascular disorders,[14] cancers, and neurodegenerative diseases. For example, recent studies have shown that CB_2R plays a fundamental role in tumorigenesis and that the CB_2R agonists may represent promising venues to develop cancer treatments.[15,16] Specifically, some of the most exciting recent research carried out by several laboratories demonstrated that CB_2R agonists potently inhibited viability, proliferation, adhesion, and migration of various cancer cells, such as breast,[17–19] prostate,[20,21] glioma,[22] colon,[23] lung,[24] thyroid,[25] lymphoma,[26] skin,[27] pancreas,[28] and liver[29] cancers. These data were collected from both cellular systems and preclinical animal models. Additional evidence indicates that the CB_2R agonists exhibit promising therapeutic value for treating neurodegenerative diseases. CB_2R agonists attenuate Alzheimer's disease pathogenesis by blocking β-amyloid peptide-induced activation of microglial cells[30] and play a neuroprotective role in Huntington's disease and amyotrophic lateral sclerosis.[31] The richness of CB_2R's regulatory roles has rendered this receptor as an attractive target to study a variety of diseases and biological processes. However, the precise role of CB_2R in the regulation of diseases remains unclear. The ability to specifically image CB_2R would contribute to develop reliable CB_2R-based therapeutic approaches with a better understanding of the mechanism of CB_2R action in these diseases.

Little has been done to target CB_2R for imaging studies and therapeutic evaluations. The current imaging techniques to identify CB_2R rely heavily on immunostaining; however, all currently available CB_2R antibodies have significant nonspecific binding issues, leading to unreliable imaging results.[6,32] As such, the development of reliable contrast agents for CB_2R imaging is critically needed in the field. Few laboratories have developed CB_2R imaging agents for positron emission tomography (PET) imaging, and CB_2R imaging using other modalities such as optical imaging has been virtually unexplored.[33] Although PET is a great imaging technique for clinical imaging and translational research due to high sensitivity and no limitation in tissue penetration, the spatial resolution is comparatively low.[34] Optical imaging is widely used for biomedical imaging due to its high sensitivity and resolution, as well as low instrument cost.[35] In clinical settings, optical imaging is a promising technology for intraoperative guidance[36–38] and optical biopsies.[39,40] Near-infrared (NIR) fluorescent dyes are typically used as the fluorophores for *in vivo* imaging applications

*Address all correspondence to: Mingfeng Bai, E-mail: baim@upmc.edu

†Zhiyuan Wu and Pin Shao equally contributed.

0091-3286/2014/$25.00

because of the relatively deep tissue penetration and negligible autofluorescence in the NIR region (650 to 900 nm).[41]

In our previous study, we reported the first CB_2R-targeted NIR fluorescent probe, NIRmbc94, which was synthesized by coupling a conjugable pyrazole-based CB_2R ligand, mbc94, with an NIR fluorescent dye, IRDye800CW.[42] We selected the pyrazole structure to develop mbc94 because SR144528, a pyrazole molecule, is a well-known selective CB_2R inverse agonist with subnanomolar binding affinity and well-characterized biology.[43] NIRmbc94 was successfully used to image CB_2R in a transfected mouse malignant astrocytoma delayed brain tumor (DBT) cell line, CB_2-mid DBT, that expresses CB_2R at endogenous levels.[44] Later on, NIRmbc94 was also used to select specific CB_2R ligands by high-throughput screening in the receptors' native environment.[45] Recently, we reported the first *in vivo* optical imaging study using another NIR fluorescent probe based on mbc94, NIR760-mbc94, which has an NIR dye (NIR760) with easy synthesis, and high fluorescence quantum yield, stability, and molar extinction coefficient.[46]

In this study, we developed a novel CB_2R-targeted NIR fluorescent probe based on a quinolone structure. Quinolone-based molecules were recently reported as highly selective CB_2R ligands with binding affinities as high as 0.2 nM.[47] To develop the quinolone-based CB_2R probe (NIR760-Q), we synthesized a novel conjugable CB_2R ligand based on the quinolone structure, followed by bioconjugation with the NIR760 dye. To demonstrate the translational potential of this new CB_2R probe, NIR760-Q was used to image CB_2R in Jurkat human acute T-lymphoblastic leukemia cells that naturally overexpress CB_2R. To our best knowledge, this is the first CB_2R-targeted cellular imaging of human cancer cells that naturally overexpress the target receptor.

2 Methods and Materials

2.1 *Synthesis of the CB_2R-Targeted NIR Probe, NIR760-Q*

The solvents used are of American Chemical Society (ACS) or high-performance liquid chromatography (HPLC) grade. The dye NIR760 and compound 3 were synthesized according to the method reported previously.[46,48,49] A Biotage (Charlotte, North Carolina) microwave reactor (model: Initiator$^+$ US/JPN 356007) was employed for the synthesis of compound 3. Flash column chromatography was run through a Teledyne Isco (Lincoln, Nebraska, combiflash RF) purification system with silica gel (standard grade, 60A, Sorbtech, Norcross, Georgia) or C18-reversed phase silica gel (20 to 40 μm, RediSepRf, Lincoln, Nebraska). ^{1}H and ^{13}C NMR spectra were recorded on a Bruker Avance (Billerica, Massachusetts) III 400-MHz NMR instrument. Mass spectra were recorded on a Waters (Milford, Massachusetts) LCT Premier mass spectrometer. UV/Vis spectra were recorded on a Cary (Santa Clara, California) 100 Bio UV-Vis spectrophotometer, and fluorescence spectra were recorded on a Cary Eclipse fluorescence spectrophotometer.

Compound 4. Under argon protection, sodium ascorbate (79 mg, 0.4 mmol) in water (1 mL) and 11-azido-3,6,9-trioxaundecan-1-amine (48 μL, 0.24 mmol) followed by copper (II) sulfate (29 mg, 0.2 mmol) in water (0.5 mL) were added to a solution of compound 3 (83 mg, 0.2 mmol) in ethanol (10 mL). The resulting reaction mixture was stirred at room temperature for 2 h and then poured into water (10 mL), followed by extraction with ethyl acetate (30 mL × 5). The organic layer was dried over anhydrous sodium sulfate and the solvent was removed by rotary evaporation. The crude product was purified by silica gel column chromatography using dichloromethane/MeOH/NH_3 H_2O (100/10/1) as the eluent. Compound 4 (0.103 g, 81%) was obtained as a colorless oil. ^{1}H NMR ($CDCl_3$): $\delta = 9.85$ (s, 1 H), 8.67 (s, 1H), 8.61 (s, 1 H), 8.38 (d, 1 H, $J = 8.8$ Hz), 8.26 (s, 1 H), 7.56 (d, 1 H, $J = 8.8$ Hz), 4.64 (br.s, 2 H), 4.22 (t, 2 H, $J = 7.2$ Hz), 3.93 (br.s, 2 H), 3.56-3.69 (m, 12 H), 2.13 (br.s, 6 H), 2.08 (br.s, 3 H), 1.84–1.87 (m, 2 H), 1.65-1.73 (m, 6 H), 1.33–1.35 (m, 4 H), 0.87 (t, 3 H, $J = 7.2$ Hz). ^{13}C NMR ($CDCl_3$): $\delta = 176.38$, 163.53, 147.31, 146.12, 138.48, 130.28, 128.06, 127.85, 123.40, 122.14, 116.89, 112.87, 70.45, 70.53, 69.57, 54.47, 51.71, 50.60, 50.51, 41.88, 36.56, 29.55, 28.84, 28.74, 22.26, 13.88. MS (ESI): calculated for $C_{35}H_{51}N_6O_5$ [M + H] m/z 635.39, found m/z 635.02.

NIR760-Q. A mixture of NIR760 (17 mg, 19 μmol), HBTU (11 mg, 29 μmol), and HOBt (3.8 mg, 28 μmol) in dry dimethylformamide (DMF) (1 mL) was stirred under argon at room temperature for 5 min. N,N-diisopropylethylamine (DIEA) (5 μL, 29 μmol) was then added and the resulting mixture was stirred for another 10 min. Next, compound 4 (12 mg, 19 μmol) in anhydrous DMF (2 mL) was added to the dye solution. The resulting mixture was stirred at room temperature in the absence of light for 20 h. The solvent was then removed by rotary evaporation and the resulting solid was purified by C18-reversed phase column chromatography using H_2O/MeOH (20% MeOH to 75% MeOH) as the eluent resulting in a relatively pure probe. The green solid was further purified by preparative HPLC using a Phenomenex Jupiter C-4 column (250 × 21.20 mm) at a flow rate of 10 mL/min. Flow A was 0.1% triethylamine (TEA) in water and flow B was 0.1% TEA in acetonitrile. The elution method started with a linear gradient from 30% to 70% B over 20 min, then from 70% to 100% B over 10 min, held at 100% B for 3 min, and finally returned to 30% B over 10 min. After being dried by lyophilization, NIR760-Q (7.1 mg, 24%) was obtained as a green solid. ^{1}H NMR (*d*6-DMSO): $\delta = 9.98$ (s, 1 H), 8.77-8.78 (m, 2 H), 8.76 (s, 1 H), 8.70 (t, 1 H, $J = 5.6$ Hz), 8.28 (dd, 1 H, $J = 2$ & 8.8 Hz), 8.12 (d, 2 H, $J = 8$ Hz), 8.00 (d, 1 H, $J = 9.2$ Hz), 7.57–7.59 (m, 4H), 7.36 (d, 2 H, $J = 8.4$ Hz), 7.33 (d, 2 H, $J = 8.4$ Hz), 7.03 (d, 2 H, $J = 13.6$ Hz), 6.41 (d, 2 H, $J = 14.4$ Hz), 4.60 (t, 2 H, $J = 4.8$ Hz), 4.46 (t, 2 H, $J = 7.2$ Hz), 4.26 (br.s, 4 H), 3.90 (t, 2 H, $J = 5.2$ Hz), 3.55-3.59 (m, 12 H), 2.71 (br.s, 4 H), 2.55 (t, 4 H, $J = 6.8$ Hz), 2.07 (br.s, 9 H), 1.90-1.97 (m, 6 H), 1.79 (br.s, 2 H), 1.67 (s, 6 H), 1.30-1.32 (m, 4 H), 1.08 (s, 12 H), 0.84 (t, 3 H, $J = 6.8$ Hz). ^{13}C NMR (*d*6-DMSO): $\delta = 175.44$, 171.35, 165.55, 162.79, 160.43, 147.83, 146.96, 145.17, 144.92, 142.20, 141.77, 139.97, 138.31, 133.76, 131.51, 129.94, 129.36, 127.62, 127.59, 127.43, 126.19, 122.52, 122.15, 119.65, 111.71, 110.14, 101.03, 69.75, 69.71, 69.62, 68.87, 68.58, 50.61, 49.73, 48.13, 47.82, 42.69, 41.70, 38.28, 36.08, 28.91, 28.44, 28.03, 27.03, 24.34, 23.26, 21.78, 13.87. MS (ESI): calculated for $C_{78}H_{96}N_8O_{18}S_4$ [M] m/z 1560.57, found m/z 1560.35.

2.2 *Reverse Transcription Polymerase Chain Reaction (RT-PCR)*

Jurkat cells were seeded into a T75 flask and cultured at 37°C for 72 h. Total ribonucleic acid (RNA) was extracted from Jurkat cells using RNAzol Reagent (Invitrogen, Grand Island, New York). Single strand cDNA was synthesized from total RNA using the SuperScript III first-strand synthesis system

(Invitrogen) for reverse transcription polymerase chain reaction (RT-PCR). Primers of CB_2R were obtained from Integrated DNA Technologies (Coralville, Iowa). The sequences used for CB_2R were 5'ccatggaggaatgctgggtg3' and 5'tcagcaatcagagaggtctag3'. Amplifications were run using Platinum® *Taq* DNA polymerase (Invitrogen) and consisted of 36 cycles of 30 s at 95°C, 60 s at 59°C, and 60 s at 69°C.

2.3 *In Vitro Saturation Binding Assay of NIR760-Q*

We carried out intact cell saturation binding assay to determine binding affinity of NIR760-Q to CB_2R. Briefly, Jurkat cells were seeded into 96 well optical bottom plates (1.5×10^5 cells per well). Cells were incubated for 30 min with an increasing concentration (0.2, 0.5, 1.0, 2.0, 5.0, 10.0, 20.0, 80.0, and 160.0 nM) of NIR760-Q at 37°C. For nonspecific binding measurements, 1 μM (final concentration) of the blocking agent 4-quinolone-3-carboxamide (4Q3C, Cayman Chemical, Ann Arbor, Michigan) was added with NIR760-Q to each well, while for total binding measurements, no blocking agent was added. Cells were then rinsed with serum free medium and the fluorescence intensity at 790 nm (relative fluorescence units) was recorded with a Synergy H4 Hybrid Multi-Mode Microplate Reader. DRAQ-5, a commonly used cell nuclear DNA labeling dye, was used to normalize cell numbers based on a fluorescence intensity at 690 nm (exited at 650 nm) using the protocol provided by the manufacturer. The specific binding was obtained by the subtraction of nonspecific binding from total binding. The dissociation constant (K_d) and receptor density (B_{max}) were estimated from the nonlinear fitting of specific binding versus NIR760-Q concentration using Prism software (GraphPad Prism 6.01, San Diego, California).

2.4 *Cell Fluorescent Imaging of NIR760-Q*

Jurkat cells were treated with 5 μM of NIR760-Q or NIR760 at 37°C for 30 min, with or without coincubation with 10 μM of 4Q3C as the blocking agent. After being washed three times with serum free medium, cells were fixed with 4% paraformaldehyde/PBS for 20 min at room temperature. The cell nucleus was stained with 1 μg/mL 4',6-diamidino-2-phenylindole (DAPI) for 15 min at room temperature. Cells were mounted and then imaged using a Zeiss (Thornwood, New York) Axio Observer fluorescent microscope equipped with the ApoTome 2 imaging system. NIR760-Q or NIR760 fluorescence images were captured using an NIR camera with ICG filter set (excitation/emission: 750 to 800 nm/820 to 875 nm). Nuclear images were obtained with a DAPI filter set (excitation/emission: 335 to 383 nm/420 to 470 nm). Differential interference contrast (DIC) images were obtained through Trans light DIC.

A multiplate reader system (Synergy H4 Hybrid) was used for the quantitative CB_2R binding assay measurements. Cells were divided into four groups: (1) Jurkat cells treated with 5 μM of NIR760-Q at 37°C for 30 min, without blocking agent; (2) Jurkat cells treated with 5 μM of NIR760-Q, together with 10 μM of 4Q3C as the blocking agent at 37°C for 30 min; (3) Jurkat cells treated with 5 μM of free NIR760 dye without targeting moiety at 37°C for 30 min; and (4) wild type DBT-cells (CB_2R-) treated with 5 μM of NIR760-Q at 37°C for 30 min. To prepare for the measurements, DBT-cells were seeded into 96-well optical plates 24 h before the treatment. Jurkat cells were grown to 90% confluence in T75 flasks, harvested, and seeded into 96-well optical plates (1.5×10^5 cells per well). Since most Jurkat cells were in suspension, the 96-well plates were centrifuged before 5 μM of NIR760-Q or NIR760 with or without 4Q3C were added in culture medium. After being incubated for 30 min, cells were washed three times with serum free medium. A Synergy H4 Hybrid Multimode Microplate Reader was used to record fluorescence intensity 790 nm (excitation at 740 nm). Assays for each group were triplicated.

2.5 *Data Processing and Statistics*

All of the data are given as the mean ± standard error of the mean of n independent measurements. Statistical analysis was performed using a two-tailed unpaired student's t test (IBM SPSS Statistics version 21), with p values <0.05 considered statistically significant.

3 Results and Discussion

The design of NIR760-Q has the following considerations: (1) The quinolone structure was chosen as the targeting moiety because certain quinolone molecules, such as 4-quinolone-3-carboxamide, were recently reported to have high CB_2R selectivity and binding affinity (K_d as high as 0.2 nM);[47] (2) A terminal amino group was introduced to the targeting moiety to allow for universal conjugation with various signaling moieties, such as fluorescent dyes (for optical imaging) and metal chelators (for PET, single photon emission-computed tomography, and magnetic resonance imaging); (3) NIR760 was selected as the fluorophore for NIR fluorescence imaging, which has high fluorescence quantum yield, stability, and molar extinction coefficient and can be synthesized with only two steps.[46] In addition, the four sulfonate groups on NIR760 introduce high hydrophilicity to the imaging probe; (4) A di(ethylene glycol) linker between the targeting moiety and NIR760 dye provides ether oxygens as hydrogen bond acceptors that can potentially facilitate the binding.[50] To synthesize NIR760-Q (Fig. 1), we first prepared quinolone compound 3 through 7-steps reactions using previously reported methods.[48,49] The following click reaction between compound 3 and 11-azido-3,6,9-trioxaundecan-1-amine provided the CB_2R ligand 4 with a terminal amine group, which was conjugated with fluorescent dye NIR760 to yield the desired probe, NIR760-Q.

Upon the synthesis of NIR760-Q, absorption and emission spectra were collected and compared with NIR760 as shown in Fig. 2. NIR760 has intense NIR absorption and emission in water with peaks at 760 and 781 nm, respectively. After conjugation with CB_2R ligand 4, the dye showed redshifted absorption and emission spectra. The maximum absorption of NIR760-Q is located at 768 nm with a high molar extinction coefficient of 2.5×10^5 M^{-1} cm^{-1}, which is comparable with that of NIR760 ($\varepsilon = 2.4 \times 10^5$ M^{-1} cm^{-1}).[46] NIR760-Q also exhibits the intense fluorescence centered at 787 nm with a high quantum yield (16.5% in water), which is roughly 60 times higher than that of indocyanine green (ICG) ($\Phi =$ 0.28% in water[51]). ICG is the only Food and Drug Administration-approved NIR fluorescent dye and typically serves as the gold standard for NIR fluorescence imaging.

We recently reported a CB_2R-targeted NIR fluorescent probe, NIR760-mbc94, which was successfully used to image CB_2R+ cells and tumors.[46] NIR760-Q and NIR760-mbc94 share the same fluorescent dye, NIR760, while the targeting molecules are based on quinolone and pyrazole structures, respectively. Compared to NIR760-mbc94, NIR760-Q has similar maximum absorption (768 versus 766 nm) and emission

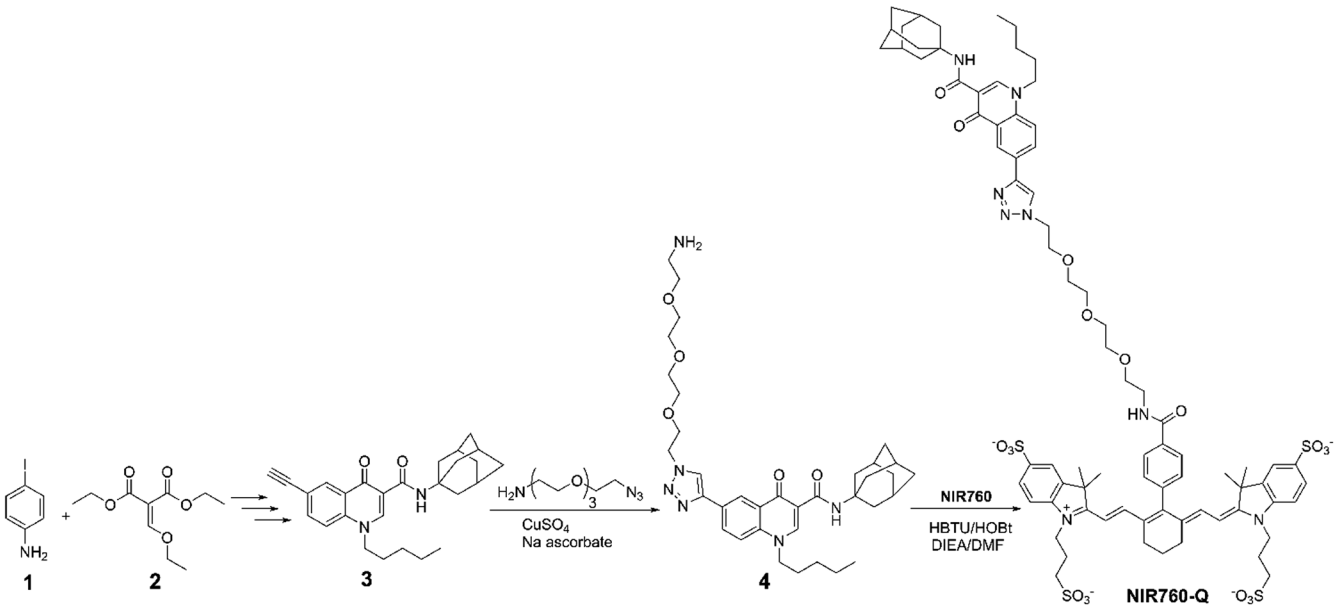

Fig. 1 Synthesis of NIR760-Q.

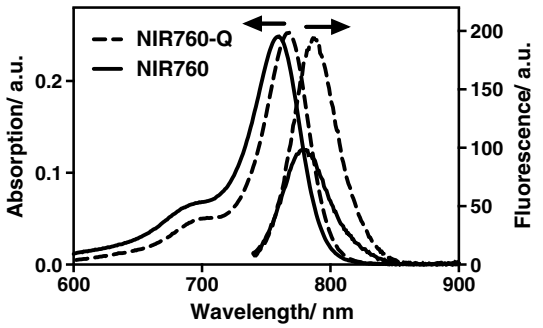

Fig. 2 The absorption and emission spectra of NIR760 (solid) and NIR760-Q (dash) in H_2O at a concentration of 1.0 μM. ($\lambda_{ex} = 720$ nm).

(787 versus 785 nm) wavelengths, but higher molar extinction coefficient ($\varepsilon = 2.5\times10^5\ M^{-1}cm^{-1}$ versus $1.44\times10^5\ M^{-1}cm^{-1}$ in water) and quantum yield ($\Phi = 16.5\%$ versus 15.2% in water). The enhanced absorption and emission near 800 nm, and excellent water solubility render NIR760-Q as an outstanding fluorescent probe for biomedical imaging.

We selected Jurkat human acute T-lymphoblastic leukemia cells to test the binding affinity and *in vitro* imaging potential of NIR760-Q. In our previous CB_2R-targeted imaging studies,[42,52] we used a transfected mouse malignant astrocytoma DBT cell line, CB_2-mid DBT, that expresses CB_2R at endogenous levels.[44] Along with CB_2-mid DBT cells, we used WT DBT cells as the CB_2R-control cells. Although CB2-DBT and WT-DBT cells are an excellent pair for studying CB_2R targeting specificity, these cells are mouse cell lines and CB_2R is not naturally expressed. To demonstrate the translational potential of the developed CB_2R-targeted probe, we used Jurkat cells that have been reported to naturally express CB_2R.[26] Before Jurkat cells were used for imaging, we verified their CB_2R expression using RT-PCR. RT-PCR was performed using primers for the human CB_2 receptor. As shown in Fig. 3, a CB_2R positive band at 1415 base pairs was detected, indicating positive mRNA expression of CB_2R in Jurkat cells.

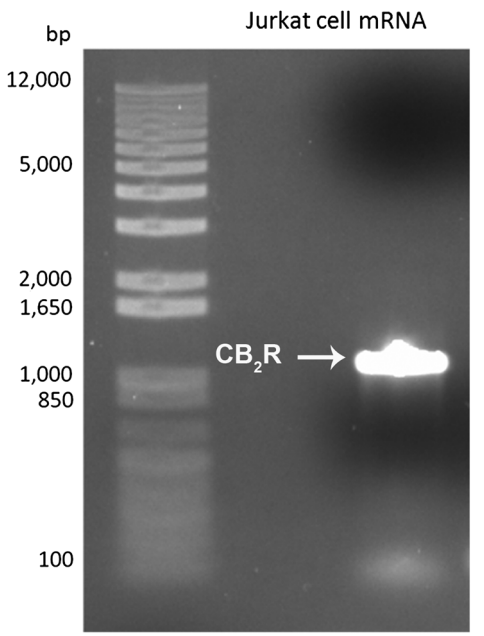

Fig. 3 CB_2R mRNA expression in Jurkat cells was assessed by RT-PCR. The band at 1415 base pairs (bp) corresponds to CB_2R.

To determine NIR760-Q's binding affinity to CB_2R in living Jurkat cells, we used an *in vitro* saturation binding assay to measure the equilibrium dissociation constant and the maximum specific binding. A large excess of 4Q3C was added to a parallel set of cells to saturate receptor binding sites and account for nonspecific binding. Figure 4 shows a representative saturation binding curve. NIR760-Q binds to CB_2R with a K_d of 75.51$\pm$ 27.97 nM and B_{max} of 440.9 $\pm$ 71.75 pmol/mg.

The CB_2R targeting specificity and imaging potential of NIR760-Q was evaluated using Jurkat cells that were incubated with 5 μM of NIR760-Q or NIR760. For blocking studies, Jurkat cells were treated with 5 μM of NIR760-Q and 10 μM of 4Q3C. We observed strong fluorescence signal from cells

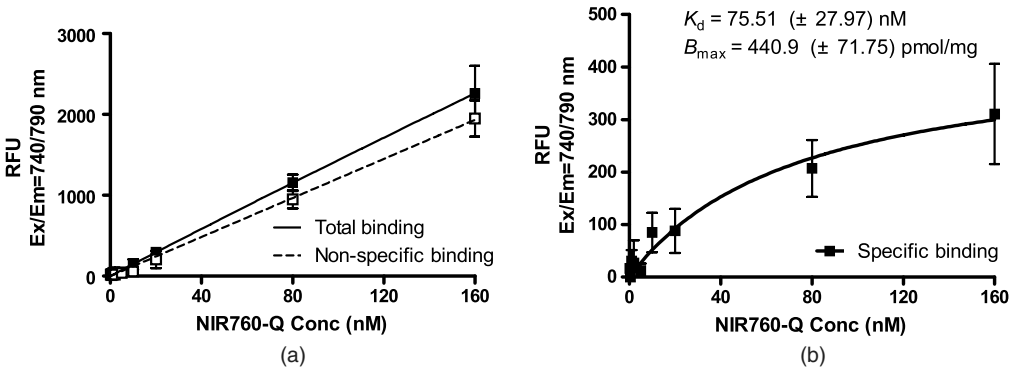

Fig. 4 *In vitro* CB_2R saturation binding assay of NIR760-Q using intact cells. (a) Total binding data (solid) were represented as relative fluorescent units (RFU) on the *y*-axis as a function of NIR760-Q concentration (*x*-axis) in the absence of 4Q3C (blocking agent). Nonspecific binding data (dash) were represented as RFU as a function of NIR760-Q concentration in the presence of 4Q3C. (b) Specific binding data were represented as RFU (*y*-axis) as a function of NIR760-Q concentration (*x*-axis). Data in *y*-axis were obtained by subtracting the nonspecific binding data from the total binding data. The dissociation constant (K_d) and receptor density (B_{max}) were estimated from the nonlinear fitting of the specific binding versus the concentration of NIR760-Q using Prism software. Each data point represents the mean ± SEM based on triplicate samples.

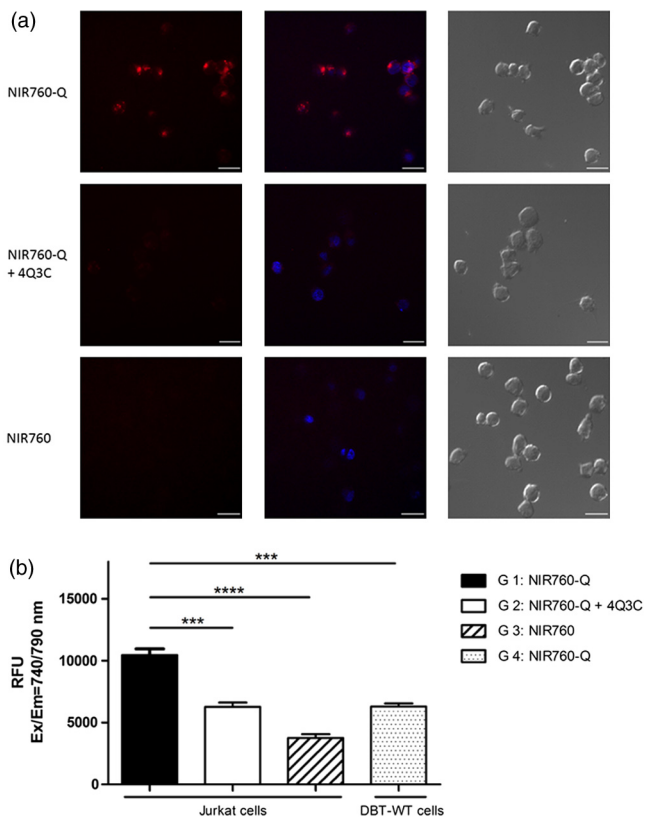

Fig. 5 NIR760-Q specifically binds to CB_2R in Jurkat cells. Jurkat cells were incubated for 30 min with 5 μM of NIR760-Q or free NIR760, with or without 10 μM of blocking agent 4Q3C. Cells were then washed three times with serum free medium before imaging. (a) Fluorescence imaging using a Zeiss Axio Observer fluorescent microscopy with ApoTome 2 imaging system. From left to right: ICG filter (red), ICG filter (red) + DAPI filter (blue) merged and differential interference contrast (DIC). Scale bar: 20 μm. (b) Quantitative fluorescent signal was measured with a Synergy H4 Hybrid Multimode Microplate Reader. Wild type DBT-cells were used as a CB_2R negative control group for comparison. Each data point represents the mean ± SEM based on triplicate samples. (***$p < 0.001$, ****$p < 0.0001$).

incubated with NIR760-Q, which primarily localized in the cytoplasm [Fig. 5(a)]. In contrast, no significant fluorescence signal was seen from cells incubated with the same concentration of free dye (NIR760) control. Moreover, challenged cells treated with both NIR760-Q and 4Q3C showed lower fluorescence signal than unchallenged cells. These results indicate specific binding of NIR760-Q to the target receptor.

To evaluate the targeting specificity of NIR760-Q in a quantitative manner, we used a multiwell plate reader system to perform Jurkat cell binding assays. Similar to the fluorescence imaging study described above, Jurkat cells were divided into three groups: (1) cells incubated with 5 μM of NIR760-Q; (2) cells incubated with 5 μM of free dye; (3) cells incubated with 5 μM of NIR760-Q and 10 μM of 4Q3C. We also used DBT-cells as the CB_2R-cell line for comparison. As shown in Fig. 5(b), Jurkat cells treated with NIR760-Q showed a 2.8-fold higher fluorescence signal than those treated with NIR760 (10469.00 ± 495.26 versus 3755.67 ± 311.81, $p < 0.0001$). Treatment with 4Q3C reduced the uptake of NIR760-Q in Jurkat cells by 40% (from 10469.00 ± 495.26 to 6274.33 ± 350.55, $p = 0.0001$). In addition, CB_2R-WT DBT cells treated with NIR760-Q showed 40% less fluorescence signal than Jurkat cells (6297.67 ± 250.68 versus 10469.00 ± 495.26, $p = 0.0001$). These results indicate specific binding of NIR760-Q to the target receptor and are consistent with our previous cellular imaging studies using NIR760-mbc94, whose uptake was also blocked by 40% when challenged with a CB_2R ligand.[46] The partial inhibition indicates nonspecific binding of NIR760-Q, which may be due to its net negative surface charge. In a recent study, Choi et al.[53] reported that replacing the negatively charged NIR fluorescent dyes with a zwitterionic dye that has no net surface charge significantly reduced the nonspecific binding of NIR fluorescent imaging probes. With a net surface charge of −4, NIR760-Q is likely to have nonspecific binding. We noticed that the cell uptake of NIR760-Q in DBT-WT cells is higher than that of NIR760 in Jurkat cells. Although both uptakes are due to nonspecific binding, the higher lipophilicity of NIR760-Q than NIR760 could have caused the enhanced level of nonspecific binding. Future study will involve developing zwitterionic CB_2R probes with reduced nonspecific

binding to allow for enhanced imaging contrast at the target site. In addition, we plan to develop a xenograft mouse model using Jurkat cells and evaluate the potential of NIR760-Q and new zwitterionic CB_2R probes *in vivo*.

4 Summary

In summary, we have developed a novel CB_2R-targeted NIR probe NIR760-Q, which demonstrated specific binding in Jurkat human cells. Compared to our previously reported CB_2R probe, NIR760-mbc94, NIR760-Q has enhanced absorption and emission and comparable binding affinity and specificity. We also report the first CB_2R-targeted optical imaging of human tumor cells that naturally express CB_2R. The combined data indicate that NIR760-Q is a promising imaging probe for CB_2R-targeted imaging with the potential of translational studies. Such an imaging tool may have great value in elucidating the regulatory role of CB_2R in various diseases.

Acknowledgments

We thank Dr. Nephi Stella at the University of Washington for providing DBT cells and technical advice. We also thank Dr. Xiangqun Xie at the University of Pittsburgh for providing support to this project. This work was supported by the startup fund provided by the Department of Radiology, University of Pittsburgh.

References

1. T. Sugiura et al., "Evidence for the involvement of the cannabinoid CB2 receptor and its endogenous ligand 2-arachidonoylglycerol in 12-O-tetradecanoylphorbol-13-acetate-induced acute inflammation in mouse ear," *J. Biol. Chem.* **280**(18), 18488–18497 (2005).
2. H. Iwamura et al., "In vitro and in vivo pharmacological characterization of JTE907, a novel selective ligand for cannabinoid CB2 receptor," *J. Pharmacol. Exp. Ther.* **296**(2), 420–425 (2001).
3. A. Makriyannis et al., "Activation of CB2 cannabinoid receptors by AM1241 inhibits experimental neuropathic pain: pain inhibition by receptors not present in the CNS," *Proc. Natl. Acad. Sci. USA* **100**(18), 10529–10533 (2003).
4. M. Karsak et al., "The cannabinoid CB2 receptor: a potential target for the diagnosis and treatment of osteoporosis," *J. Bone Miner. Res.* **19**(S1), S383–S383 (2004).
5. R. G. Pertwee, "Cannabinoids and multiple sclerosis," *Mol. Neurobiol.* **36**(1), 45–59 (2007).
6. M. Morales and A. Bonci, "Hooking CB2 receptor into drug abuse?," *Nat. Med.* **18**(4), 504–505 (2012).
7. I. Gamaleddin et al., "Effects of a selective cannabinoid CB2 agonist and antagonist on intravenous nicotine self administration and reinstatement of nicotine seeking," *Plos One* **7**(1), e29900 (2012).
8. A. Ortega-Alvaro et al., "Deletion of CB2 cannabinoid receptor induces schizophrenia-related behaviors in mice," *Neuropsychopharmacology* **36**(7), 1489–1504 (2011).
9. M. S. Garcia-Gutierrez and J. Manzanares, "Overexpression of CB2 cannabinoid receptors decreased vulnerability to anxiety and impaired anxiolytic action of alprazolam in mice," *J. Psychopharmacol.* **25**(1), 111–120 (2011).
10. M. S. Garcia-Gutierrez et al., "Chronic blockade of cannabinoid CB2 receptors induces anxiolytic-like actions associated with alterations in GABA(A) receptors," *Br. J. Pharmacol.* **165**(4), 951–964 (2012).
11. K. A. Jenkin et al., "Endocannabinoids and the renal proximal tubule: an emerging role in diabetic nephropathy," *Int. J. Biochem. Cell Biol.* **44**(11), 2028–2031 (2012).
12. J. Agudo et al., "Deficiency of CB2 cannabinoid receptor in mice improves insulin sensitivity but increases food intake and obesity with age," *Diabetologia* **53**(12), 2629–2640 (2010).
13. C. Gonzalez et al., "Cannabinoid/agonist WIN 55,212-2 reduces cardiac ischaemia—reperfusion injury in Zucker diabetic fatty rats: role of CB2 receptors and iNOS/eNOS," *Diabetes-Metab. Res.* **27**(4), 331–340 (2011).
14. S. Steffens and P. Pacher, "Targeting cannabinoid receptor CB2 in cardiovascular disorders: promises and controversies," *Br. J. Pharmacol.* **167**(2), 313–323 (2012).
15. G. Velasco et al., "Cannabinoids and gliomas," *Mol. Neurobiol.* **36**(1), 60–67 (2007).
16. P. Pacher, S. Batkai, and G. Kunos, "The endocannabinoid system as an emerging target of pharmacotherapy," *Pharmacol. Rev.* **58**(3), 389–462 (2006).
17. Z. Qamri et al., "Synthetic cannabinoid receptor agonists inhibit tumor growth and metastasis of breast cancer," *Mol. Cancer Ther.* **8**(11), 3117–3129 (2009).
18. M. M. Caffarel et al., "Cannabinoids: a new hope for breast cancer therapy?," *Cancer Treat Rev.* **38**(7), 911–918 (2012).
19. M. M. Caffarell et al., "Antitumoural effect of cannabinoids in an animal model of breast cancer," *EJC Suppl.* **6**(9), 18–18 (2008).
20. N. Olea-Herrero et al., "Inhibition of human tumour prostate PC-3 cell growth by cannabinoids R(+)-Methanandamide and JWH-015: involvement of CB2," *Br. J. Cancer* **101**(6), 940–950 (2009).
21. S. Sarfaraz et al., "Cannabinoid receptor as a novel target for the treatment of prostate cancer," *Cancer Res.* **65**(5), 1635–1641 (2005).
22. C. Sanchez et al., "Inhibition of glioma growth in vivo by selective activation of the CB2 cannabinoid receptor," *Cancer Res.* **61**(15), 5784–5789 (2001).
23. F. Cianchi et al., "Cannabinoid Receptor activation induces apoptosis through tumor necrosis factor alpha—mediated ceramide de novo synthesis in colon cancer cells," *Clin. Cancer Res.* **14**(23), 7691–7700 (2008).
24. A. Preet et al., "Cannabinoid receptors, CB1 and CB2, as novel targets for inhibition of non-small cell lung cancer growth and metastasis," *Cancer Prev. Res.* **4**(1), 65–75 (2011).
25. Y. Shi et al., "Cannabinoid 2 receptor induction by IL-12 and its potential as a therapeutic target for the treatment of anaplastic thyroid carcinoma," *Cancer Gene Ther.* **15**(2), 101–107 (2008).
26. R. J. McKallip et al., "Targeting CB2 cannabinoid receptors as a novel therapy to treat malignant lymphoblastic disease," *Blood* **100**(2), 627–634 (2002).
27. C. Blazquez et al., "Cannabinoid receptors as novel targets for the treatment of melanoma," *Faseb. J.* **20**(14), 2633–2635 (2006).
28. A. Carracedo et al., "Cannabinoids induce apoptosis of pancreatic tumor cells via endoplasmic reticulum stress-related genes," *Cancer Res.* **66**(13), 6748–6755 (2006).
29. D. Vara et al., "Anti-tumoral action of cannabinoids on hepatocellular carcinoma: role of AMPK-dependent activation of autophagy," *Cell Death Differ.* **18**(7), 1099–1111 (2011).
30. B. G. Ramirez et al., "Prevention of Alzheimer's disease pathology by cannabinoids: neuroprotection mediated by blockade of microglial activation," *J. Neurosci.* **25**(8), 1904–1913 (2005).
31. E. L. Scotter, M. E. Abood, and M. Glass, "The endocannabinoid system as a target for the treatment of neurodegenerative disease," *Br. J. Pharmacol.* **160**(3), 480–498 (2010).
32. E. Torres et al., "Evidence that MDMA ('ecstasy') increases cannabinoid CB2 receptor expression in microglial cells: role in the neuroinflammatory response in rat brain," *J. Neurochem.* **113**(1), 67–78 (2010).
33. N. Evens and G. M. Bormans, "Non-invasive imaging of the type 2 cannabinoid receptor, focus on positron emission tomography," *Curr. Top. Med. Chem.* **10**(15), 1527–1543 (2010).
34. T. F. Massoud and S. S. Gambhir, "Molecular imaging in living subjects: seeing fundamental biological processes in a new light," *Gene Dev.* **17**(5), 545–580 (2003).
35. J. V. Frangioni, "In vivo near-infrared fluorescence imaging," *Curr. Opin. Chem. Biol.* **7**(5), 626–634 (2003).
36. L. M. A. Crane et al., "Intraoperative near-infrared fluorescence imaging for sentinel lymph node detection in vulvar cancer: first clinical results," *Gynecol. Oncol.* **120**(2), 291–295 (2011).
37. G. M. van Dam et al., "Intraoperative tumor-specific fluorescence imaging in ovarian cancer by folate receptor-alpha targeting: first in-human results," *Nat. Med.* **17**(10), 1315–U1202 (2011).
38. A. G. T. T. van Scheltinga et al., "Intraoperative near-infrared fluorescence tumor imaging with vascular endothelial growth factor and human epidermal growth factor receptor 2 targeting antibodies," *J. Nucl. Med.* **52**(11), 1778–1785 (2011).

39. R. Atreya, M. J. Waldner, and M. F. Neurath, "Molecular imaging: interaction between basic and clinical science," *Gastroenterol. Clin. North. Am.* **39**(4), 911–922 (2010).
40. H. K. Roy et al., "Colonoscopy and optical biopsy: bridging technological advances to clinical practice," *Gastroenterology* **140**(7), 1863–1867 (2011).
41. M. Bai and D. J. Bornhop, "Recent advances in receptor-targeted fluorescent probes for in vivo cancer imaging," *Curr. Med. Chem.* **19**(28), 4742–4758 (2012).
42. M. F. Bai et al., "MBC94, a conjugable ligand for cannabinoid CB2 receptor imaging," *Bioconjugate Chem.* **19**(5), 988–992 (2008).
43. R. G. Pertwee and R. A. Ross, "Cannabinoid receptors and their ligands," *Prostaglandins, Leukot. Essent. Fatty Acids* **66**(2–3), 101–121 (2002).
44. E. Cudaback et al., "The expression level of CB1 and CB2 receptors determines their efficacy at inducing apoptosis in astrocytomas," *Plos One* **5**(1), e8702 (2010).
45. M. Sexton et al., "NIR-mbc94, a fluorescent ligand that binds to endogenous CB(2) receptors and is amenable to high-throughput screening," *Chem. Biol.* **18**(5), 563–568 (2011).
46. S. Zhang, P. Shao, and M. Bai, "In vivo Type 2 cannabinoid receptor-targeted tumor optical imaging using a near infrared fluorescent probe," *Bioconjug. Chem.* **24**(11), 1907–1916 (2013).
47. S. Pasquini et al., "Investigations on the 4-quinolone-3-carboxylic acid motif. 4. identification of new potent and selective ligands for the cannabinoid type 2 receptor with diverse substitution patterns and antihyperalgesic effects in mice," *J. Med. Chem.* **54**(15), 5444–5453 (2011).
48. S. Pasquini et al., "Investigations on the 4-Quinolone-3-carboxylic acid motif. 3. Synthesis, structure-affinity relationships, and pharmacological characterization of 6-substituted 4-quinolone-3-carboxamides as highly selective cannabinoid-2 receptor ligands," *J. Med. Chem.* **53**(16), 5915–5928 (2010).
49. S. Pasquini et al., "Investigations on the 4-quinolone-3-carboxylic acid motif. 2. Synthesis and structure-activity relationship of potent and selective cannabinoid-2 receptor agonists endowed with analgesic activity in vivo," *J. Med. Chem.* **51**(16), 5075–5084 (2008).
50. B. Schafer et al., "Preparation of semisynthetic lipoproteins with fluorescent cholesterol anchor and their introduction to the cell membrane with minimal disruption of the membrane," *Bioconjug. Chem.* **24**(10), 1684–1697 (2013).
51. R. C. Benson and H. A. Kues, "Fluorescence properties of indocyanine green as related to angiography," *Phys. Med. Biol.* **23**(1), 159–163 (1978).
52. Y. Zhang et al., "Imaging tumor angiogenesis in breast cancer experimental lung metastasis with positron emission tomography, near-infrared fluorescence, and bioluminescence," *Angiogenesis* **16**(3), 663–674 (2013).
53. H. S. Choi et al., "Targeted zwitterionic near-infrared fluorophores for improved optical imaging," *Nat. Biotechnol.* **31**(2), 148–153 (2013).

Zhiyuan Wu received his MD degree from Shanghai Jiao Tong University School of Medicine, China, and is currently working as a postdoctoral fellow in Dr. Mingfeng Bai's lab at the University of Pittsburgh. His research interests include molecular imaging of cancer and imaging biomarkers research. He has published more than 40 peer-reviewed journal articles in these fields.

Pin Shao is currently a research associate in Dr. Mingfeng Bai's lab at the Department of Radiology, University of Pittsburgh. She obtained her PhD degree in chemistry from Wuhan University, China, and her research interests are in the development of novel near-infrared fluorescent compounds for optical and/or photoacoustic imaging, as well as drug delivery.

Shaojuan Zhang earned her PhD degree at Gunma University, Japan, and is currently a postdoctoral fellow at the University of Pittsburgh, under the mentorship of Dr. Mingfeng Bai. Her research interests are targeted optical imaging and cancer therapeutics using molecular probes.

Xiaoxi Ling earned his PhD degree in chemistry from Ohio University and is currently a postdoctoral fellow in Dr. Mingfeng Bai's Lab at the University of Pittsburgh. His research involves the development of near-infrared fluorescence imaging probes and theranostic agents.

Mingfeng Bai is an assistant professor of radiology at the University of Pittsburgh. He received his MSc and PhD degrees in chemistry from Vanderbilt University and BS degree in chemistry from Nankai University, China. His research group is focused on developing novel molecular imaging probes for diagnostic imaging and phototherapy. He has published peer-reviewed journal articles, holds various patents, and has given many presentations nationally and internationally.